INTERNATIONAL JOURNAL OF CLIMATOLOGY
Int. J. Climatol. (2014)
Published online in Wiley Online Library
(wileyonlinelibrary.com) DOI: 10.1002/joc.4043

RMetS
Royal Meteorological Society

Projected changes in temperature and precipitation in ten river basins over China in 21st century

Qiaohong Sun, Chiyuan Miao* and Qingyun Duan
State Key Laboratory of Earth Surface Processes and Resource Ecology, College of Global Change and Earth System Science, Beijing Normal University, P.R. China

ABSTRACT: Present and future climate change information is required to develop adaptation and mitigation strategies at national and international levels. This study assessed the simulated surface air temperature (SAT) and precipitation (PR) over China from 24 models involved in the Coupled Model Intercomparison Project Phase 5 (CMIP5). The reliability ensemble average (REA) is applied to project the SAT and PR change under representative concentration pathway (RCP) scenarios over China in the 21st century. The results show that most CMIP5 models tend to underestimate SAT and overestimate PR in China. Models generally agree better with the observed SAT than PR. For SAT, the ensemble prediction shows that warming is expected all over China for all RCPs. The warming trend from 2006 to 2099 in China is 0.87 ± 0.14 °C 100 year^{-1}, 2.47 ± 0.48 °C 100 year^{-1}, 5.85 ± 0.73 °C 100 year^{-1} for RCP 2.6, RCP 4.5 and RCP 8.5, respectively. Northern regions experience more warming than southern regions. The Songhua River basin warms the most, considering the ten studied basins for RCP 4.5 and RCP 8.5. Under RCP 2.6, the largest warming trend occurs in the Huaihe River basin. For PR, the spatial pattern of PR change has zonal characteristics. The girds with the maximum linear trend, i.e. >7.5 mm decade^{-1}, are concentrated in the upper Yangtze River basin. For temporal scale, PR in China is also projected to increase during the 21st century by $4.89 \pm 2.30\%$ 100 year^{-1}, $8.67 \pm 6.27\%$ 100 year^{-1} and $13.39 \pm 12.58\%$ 100 year^{-1} for RCP 2.6, RCP 4.5 and RCP 8.5, respectively. PR tends to decrease in the Yangtze River basin, Southeast River Drainage and Pearl River basin during the early period (2011–2030) for all RCPs, largely increase thereafter. However, uncertainties are unavoidable for SAT and PR projections. The PR uncertainty exceeds the temperature uncertainty. More studies regarding the analysis of narrowing uncertainties are essential for a better understanding of climate change.

KEY WORDS multi-model ensembles; reliability; China; CMIP5

Received 12 November 2013; Revised 12 April 2014; Accepted 16 April 2014

1. Introduction

It is generally accepted that global climate has changed, caused by increasing atmospheric carbon dioxide (CO_2) and other greenhouse trace gas concentrations and anthropogenic activities (IPCC, 2001). Climate change has inevitable effects on biological, physical and socio-economic processes. Present and future climate change information at global, regional and local scales is required to develop national- and international-level adaptation and mitigation strategies (Xu *et al.*, 2010; Miao *et al.*, 2011). Due to the progresses in modelling and understanding of the climate system physical processes, the general circulation model (GCM) has gradually become a primary tool for climate change research (IPCC, 2007). Driven by different radiative forcings, GCMs can simulate present-day climate and project future climate conditions under different scenarios (IPCC, 1990; Li *et al.*, 2011; McAfee *et al.*, 2011; Xu *et al.*, 2011; Miao *et al.*, 2013; Ou *et al.*, 2013).

The World Climate Research Program (WCRP) developed the Coupled Model Intercomparison Project (CMIP), which provides coordinated simulations from the state-of-the-art global climate models. The project provides an opportunity for model comparison and multi-model ensemble strategy development (Li *et al.*, 2011). Climate models are not perfect because the theoretical understanding of climate remains incomplete, and certain simplifying assumptions are unavoidable when formulating these models (Reichler and Kim, 2008). Recent studies have shown that the model agreement with present-day observations is currently the only way to determine model quality (IPCC, 2001); good model performance evaluated from the present climate guarantees the higher reliability of climate change simulations to some extent (Giorgi and Mearns, 2002; Coquard *et al.*, 2004). Various studies have attempted to assess the performance of climate models in simulating the present-day climate and to predict the future climate on continental and regional scales (Lambert and Boer, 2001; Duan and Phillips, 2010; Scherrer, 2011; Miao *et al.*, 2012a; Grainger *et al.*, 2013; Sillmann *et al.*, 2013; Wu *et al.*, 2013). The results have shown that many coupled global climate models have increasingly performed

* Correspondence to: C. Miao, State Key Laboratory of Earth Surface Processes and Resource Ecology, College of Global Change and Earth System Science, Beijing Normal University, Beijing 100875, P.R. China.
E-mail: miaocy@vip.sina.com

well in simulating climate changes due to extensive model development (Zhou and Yu, 2006; Reichler and Kim, 2008; Annan and Hargreaves, 2010). However, not all GCMs are similarly able to represent accurate climate characteristics (Coquard *et al.*, 2004; Phillips and Gleckler, 2006; Räisänen, 2007; Giorgi and Coppola, 2010), and forecasts of climate change are inevitably uncertain (Allen *et al.*, 2000).

To reduce the simulation uncertainly and improve GCM predictions, many studies have adopted multi-model ensemble techniques. It is generally accepted that the model uncertainties may be reduced and the model credibility can be improved by employing multi-model ensembles (Feng *et al.*, 2010). Many studies have also simulated historical climate with respect to observations. Generally, the performance of multi-model ensembles is often found to be better than the individual simulation (Krishnamurti, 2000; IPCC, 2001; Duan and Phillips, 2010). A possible explanation is that the multi-model ensemble embraces distinctly different physical parameterizations, thus surmounting the limitations of an overconfident single-model simulation (Duan and Phillips, 2010). Hence, ensembles can be used to produce more reliable predictions (Tebaldi and Knutti, 2007).

Giorgi and Mearns (2002) developed the reliability ensemble averaging (REA) methodology that produces a weighted average of climate change ensemble results based on the 'reliability' of each model. 'Reliability' considers the ability of a particular model to simulate the observed climate and its degree of convergence in predicted climate change compared with the other ensemble members. The REA method also assesses the reliability of the projected weighted average climate change, allowing PDFs for climate variables in climate change conditions to be determined (Giorgi and Mearns, 2002; Giorgi, 2003). Many previous studies have applied the method for the evaluation and projection of climate change in different regions. For example, Moise and Hudson (2008) applied the method to a multi-model ensemble of coupled atmosphere–ocean general circulation models (AOGCMs) from the third phase of CIMP (CMIP3) to produce mean and probabilistic climate change projections for Australia and southern Africa. Mote and Salathé (2010) analysed the future climate in the Pacific Northwest for each season and the annual mean based on REA results. Giraldo Osorio and García Galiano (2011) applied the REA method to assess the ability of the regional climate models (RCMs) to reproduce the present-day climate and to evaluate the convergence of different RCMs for a given forcing scenario in the Senegal River basin. Furthermore, Tao *et al.* (2012) presented projected precipitation and temperature changes in the Yangtze River basin from a 20-member ensemble mean. Torres and Marengo (2013) utilized the REA method to assess the uncertainties involved in projections of seasonal temperature and precipitation changes over South America in the 21st century.

China is a large agricultural country with a large fraction of the world's land. The climate in China varies greatly over space and time due to the pronounced topographical gradients and complexity (Gao *et al.*, 2008). Temperature and precipitation changes have a major effect on the runoff of river basins, water cycle and the safety of the water supply (Miao *et al.*, 2010, 2012b). Nevertheless, there are not enough studies carried out to comprehensively assess the spatio-temporal changes for all of the river basins in China in 21st century. The information is required to assess the effect of climate change on the spatial and temporal distributions of water resources and to develop adaptation and mitigation strategies according to different regions. Moreover, the fifth experiment of CIMP (CMIP5), used for the Intergovernmental Panel on Climate Change (IPCC) fifth assessment report, is now available. Compared with the previous experiment of the CMIP, extensive efforts have been put forth in CMIP5, including a larger number of more complex models run at higher resolution, with more complete 'representative concentration pathways' (RCPs) of external forcings, more scenarios and more saved diagnostics (Moss *et al.*, 2010; Taylor *et al.*, 2012). Thus, the goal of this study is to (1) assess the performance of the CMIP5 GCMs in simulating precipitation and temperature variation over China and (2) project the temperature and precipitation change under different concentrations or emission scenarios in different river basins of China in the 21st century.

2. Data and methods

2.1. Data

Monthly surface air temperature (SAT) and precipitation (PR) observations for China were obtained from the National Meteorological Information Center, China Meteorological Administration (CN05) (Xu *et al.*, 2009) and the gauge-based analysis of daily precipitation over East Asia (EA) (Xie *et al.*, 2007), respectively. The EA data set is a combination of more than 2200 gauge observations (Figure 1(a)), and CN05 is based on interpolated data from 751 observing stations in China (Sun *et al.*, 2014). The data set resolutions are both $0.5° \times 0.5°$.

Monthly SAT and PR from 24 IPCC AR5 CMIP5 models (Taylor *et al.*, 2012) were used in this study (Table 1, available at http://pcmdi9.llnl.gov/esgf-web-fe/). Model results from historical simulations (1962–2005) and future climate projections (2006–2099) under different scenarios were used. Unlike the Special Report on Emissions Scenarios (SRES) B1, A1B and A2 used in CMIP3, CMIP5 uses the new RCPs. The RCPs are named according to their radiative forcing level in 2100, i.e. RCP 8.5 corresponds to a radiative forcing of $8.5\ \mathrm{W\,m^{-2}}$ in 2100. The three main future scenarios, i.e. RCP 2.6, RCP 4.5 and RCP 8.5, were involved in this research. The CMIP5 models have different spatial resolutions. To provide fair comparison with observations, all model data were interpolated to a common $0.5° \times 0.5°$ grid. Moreover, 1970–1999 was selected as the baseline period.

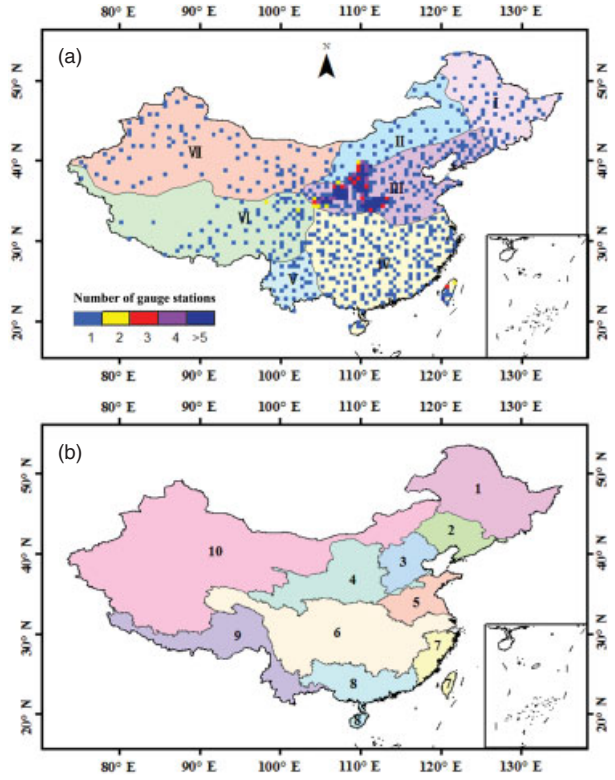

Figure 1. Location of the climatic divisions, main river basins and the number of gauge stations in a 0.5° latitude–longitude grid. The roman numerals in (a) denote the climate regions: I, northeast China (NEC); II, Inner Mongolia (IM); III, north China (NC); IV, south-central China (SCC); V, southwest China (SW); VI, Qinghai-Tibet Plateau region (QT); VII, northwest China (NWC). The numbers in (b) denote the river catchments: 1, Songhua River; 2, Liaohe River; 3, Haihe River; 4, Yellow River; 5, Huaihe River; 6, Yangtze River; 7, Southeast River Drainage; 8, Pearl River; 9, Southwest River Drainage; 10, Northwest River Drainage.

2.2. Analysis methods

2.2.1. *Skill score*

In analysing the simulated SAT and PR patterns from 1962 to 2005, two skill score metrics were used to evaluate the overall agreement between the predictions P and the observations O. The first metric is the Pearson correlation coefficient (R), which quantifies similarities between the spatial and temporal patterns of the predicted and observed values:

$$R = \frac{\sum_{i=1}^{n}\left(P_i - \overline{P}\right)\left(O_i - \overline{O}\right)}{\sqrt{\sum_{i=1}^{n}\left(P_i - \overline{P}\right)^2} \times \sqrt{\sum_{i=1}^{n}\left(O_i - \overline{O}\right)^2}} \quad (1)$$

where i represents the number of grids when quantifying the spatial patterns, but means the number of time when quantifying the temporal patterns. R is between -1 and 1. In general, $R \sim 1$ implies a close match between the (spatial or temporal) simulated and observed climate characteristics, and $R \sim 0$ indicates a lack of similarity. Moreover, for $R \sim -1$, the respective simulated and observed fields are similar however inversely proportional.

The second metric is the root-mean-square error (RMSE) between the simulated and observed data:

$$\mathrm{RMSE} = \sqrt{\frac{1}{n}\sum_{i=1}^{n}\left(P_i - O_i\right)^2} \quad (2)$$

where the sum is calculated for n spatial grid points (or temporal units). Therefore, as the RMSE gets smaller, the difference between the point-wise magnitudes of the simulated and observed climate characteristics decreases.

The third metric is the Taylor diagram, which can provide a concise statistical summary of how well patterns match between simulation and observation in terms of their correlation (R), their root-mean-square difference (RMSD) and the ratio of their variances (Taylor, 2001). The radial distance from the origin is proportional to the standard deviation of a pattern. The correlation between the simulation and observation is given by the azimuthal position of the test field. The RMSD is defined by Taylor (2001):

$$\mathrm{RMSD}^2 = \sigma_\mathrm{p}^2 + \sigma_0^2 - 2\sigma_\mathrm{p}\sigma_o R \quad (3)$$

where σ_p and σ_o are the standard deviations of the simulations and observation, respectively. The RMSD between the simulation and observation field is proportional to their distance apart (in the same units as the standard deviation).

2.2.2. *REA method*

The REA method was adopted to project the changes of PR and SAT during 2006–2099 under the three RCP scenarios (i.e. RCP 2.6, RCP 4.5 and RCP 8.5). Considering that regional climate in China is largely different, we calculated the REA weight based on the climatic division map for China (Figure 1(a)) (Ren *et al.*, 1985). To better understand hydrological processes, climate change in ten river basins (Cong *et al.*, 2010; Zhai *et al.*, 2010; Liu *et al.*, 2012; Figure 1(b)) under the future scenarios was compared and analysed. The SAT and PR were projected in the 21st century over China and the ten river basins (Figure 1(b)) using these weights.

REA uses a bias factor and a distance factor to weight each model's output. The weights are defined by Giorgi and Mearns (2002):

$$W_i = \left[\left(R_{B,i}\right)^m \times \left(R_{D,i}\right)^n\right]^{[1/(m\times n)]} = \left[\left(\frac{\epsilon_T}{|B_{T,i}|}\right)^m \times \left(\frac{\epsilon_T}{|D_{T,i}|}\right)^n\right]^{[1/(m\times n)]} \quad (4)$$

The weighted ensemble average is computed for separate subcontinental regions as

$$\Delta\breve{T} = \frac{\sum_i W_i \Delta T_i}{\sum_i W_i} \quad (5)$$

where the individual model projections of change are indicated by ΔT_i. The weight for an individual model is W_i, defined as the product of two terms, i.e. $R_{B,i}$ and $R_{D,i}$; one inversely proportional to the absolute bias, $B_{T,i}$ and the

Table 1. The CMIP5 models for which historical, RCP 2.6, RCP 4.5 and RCP 8.5 results were available from the Earth System Grid (ESG).

GCM	Model	Source	Resolution (longitude × latitude)
1	BCC-CSM 1.1	Beijing Climate Center, China Meteorological Administration, China	2.812° × 2.812°
2	BCC-CSM 1.1(m)	Beijing Climate Center, China Meteorological Administration, China	1.125° × 1.125°
3	BNU-ESM	Beijing Normal University, China	2.812° × 2.812°
4	CanESM2	Canadian Centre for Climate Modelling and Analysis, Canada	2.812° × 2.812°
5	CNRM-CM5	Centre National de Recherches Meteorologiques, Meteo-France, France	1.406° × 1.406°
6	CSIRO-Mk3.6.0	Australian Commonwealth Scientific and Industrial Research Organization, Australia	1.875° × 1.875°
7	CCSM4	National Center for Atmospheric Research (NCAR), USA	1.25° × 1.25°
8	FIO-ESM	The First Institute of Oceanography, SOA, China	2.812° × 2.812°
9	GFDL-CM3	Geophysical Fluid Dynamics Laboratory, USA	2.5° × 2.0°
10	GFDL-ESM2G	Geophysical Fluid Dynamics Laboratory, USA	2.5° × 2.0°
11	GISS-E2-H	NASA Goddard Institute for Space Studies, USA	2.5° × 2.0°
12	GISS-E2-R	NASA Goddard Institute for Space Studies, USA	2.5° × 2.0°
13	HadGEM2-ES	Met Office Hadley Centre, UK	1.241° × 1.875°
14	IPSL-CM5A-LR	Institut Pierre-Simon Laplace, France	3.75° × 1.875°
15	IPSL-CM5A-MR	Institut Pierre-Simon Laplace, France	2.5° × 1.259°
16	MPI-ESM-LR	Max Planck Institute for Meteorology, Germany	1.875° × 1.875°
17	MPI-ESM-MR	Max Planck Institute for Meteorology, Germany	1.875° × 1.875°
18	MIROC-ESM	AORI, NIES, JAMSTEC, Japan	2.812° × 2.812°
19	MIROC-ESM-CHEM	AORI, NIES, JAMSTEC, Japan	2.812° × 2.812°
20	MIROC5	Atmosphere and Ocean Research Institute (The University of Tokyo), National Institute for Environmental Studies, and Japan Agency for Marine-Earth Science and Technology, Japan	1.406° × 1.406°
21	MRI-CGCM3	Meteorological Research Institute, Japan	1.125° × 1.125°
22	NorESM1-M	Norwegian Climate Centre, Norway	2.5° × 1.875°
23	NorESM1-ME	Norwegian Climate Centre, Norway	2.5° × 1.875°
24	FGOALS-g2	Institute of Atmospheric Physics, Chinese Academy of Sciences, China	2.812° × 3.0°

other to the absolute distance between the model projected change and the final weighted ensemble average, $D_{T,i}$, respectively. Moreover, ϵ_T is a measure of natural variability, ensuring that models with small bias and deviations relative to natural fluctuations would not be unjustly discounted. We computed time series of observed regionally averaged SAT and PR for the period 1962–2006 within seven climatic divisions (Figure 1(a)) using the CN05 and EA data sets. Then, we computed 10-year moving averages after linearly detrending the data. In addition, ϵ_T was estimated to be the difference between the 10-year moving average maximum and minimum values. The exponent m and n can modulate the relative importance of the two terms in the weighted average and are equivalent in this study (Giorgi and Mearns, 2002; Giraldo and García Galiano, 2011). Through the parameters defined above, the uncertainty range around the REA mean change ($\breve{\delta}_{\Delta T}$) can be estimated by

$$\breve{\delta}_{\Delta T} = \left[\frac{\sum_i R_i \left(\Delta T_i - \Delta \breve{T} \right)^2}{\sum_i R_i} \right]^{1/2} \tag{6}$$

The upper and lower uncertainty limits are thus defined by

$$\Delta T_+ = \Delta \breve{T} + \breve{\delta}_{\Delta T} \tag{7a}$$

$$\Delta T_- = \Delta \breve{T} - \breve{\delta}_{\Delta T} \tag{7b}$$

Thus the total uncertainty range is give by $\Delta T_+ - \Delta T_- = 2\breve{\delta}_{\Delta T}$. Specific details of the REA process are provided by Giorgi and Mearns (2002).

3. Results

3.1. Comparison of model simulations with observations

3.1.1. Temporal simulations

Figure 2 shows box plots of the observed and simulated average SAT and PR over ten river basins and China. For SAT, most models tend to underestimate the annual mean SAT over different basins and China. The MIROC5 and MIROC-ESM-CHEM models always overestimate the annual mean SAT in all basins. Moreover, the CSIRO-Mk3.6.0 model gives the highest cold bias in Yellow River basin, Yangtze River basin and Southwest River drainage system compared observations and other models. However, in Songhua River basin, Haihe River basin, Northwest River drainage system and China, the FGOALS-g2 model has the lowest annual mean SAT. In all river basins, the biases of the ensemble results based on the REA method are relatively lower. For PR, except Southeast River drainage system and Pearl River basin, almost all models overestimate the annual mean PR in other

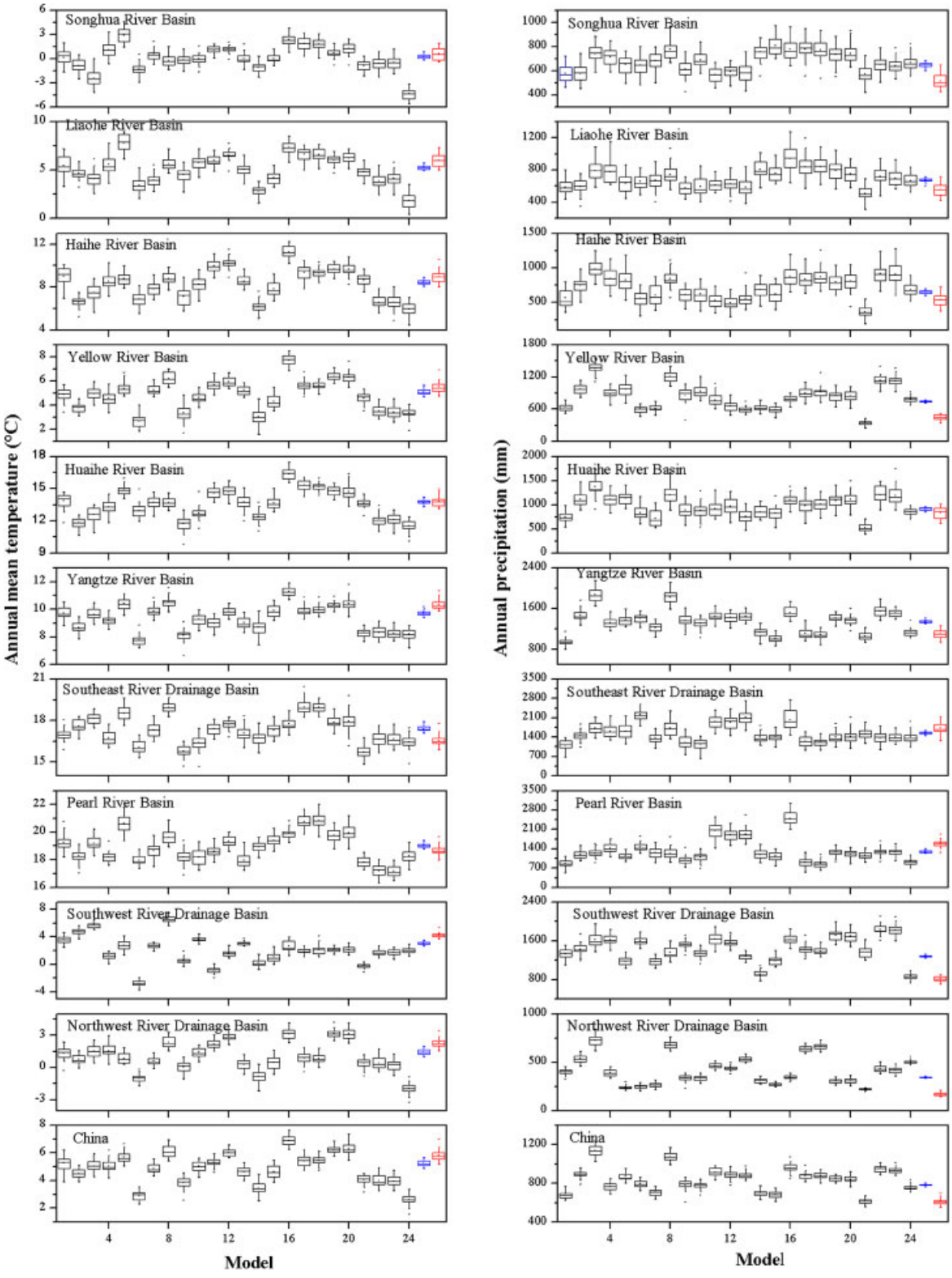

Figure 2. Box plots of the observed and simulated average temperature (left) and precipitation (right) for the period 1970–1999 in the ten river basins and China. The coloured boxes indicate the mean climatological variables outputted by single GCM (black), multi-model ensemble mean (blue) and observation (red).

river basin and over China compared with the observations. The BNU-ESM model predicts the maximum biases in Haihe River basin, Yellow River basin, Huaihe River basin, Yangtze River basin and Northwest River drainage system. The ensemble mean overestimates PR in all regions except Southeast River drainage system and Pearl River basin.

Figure 3 shows the correlation coefficient (R) and RMSE between simulation and observation. The simulation comes from 24 models and REA results, the

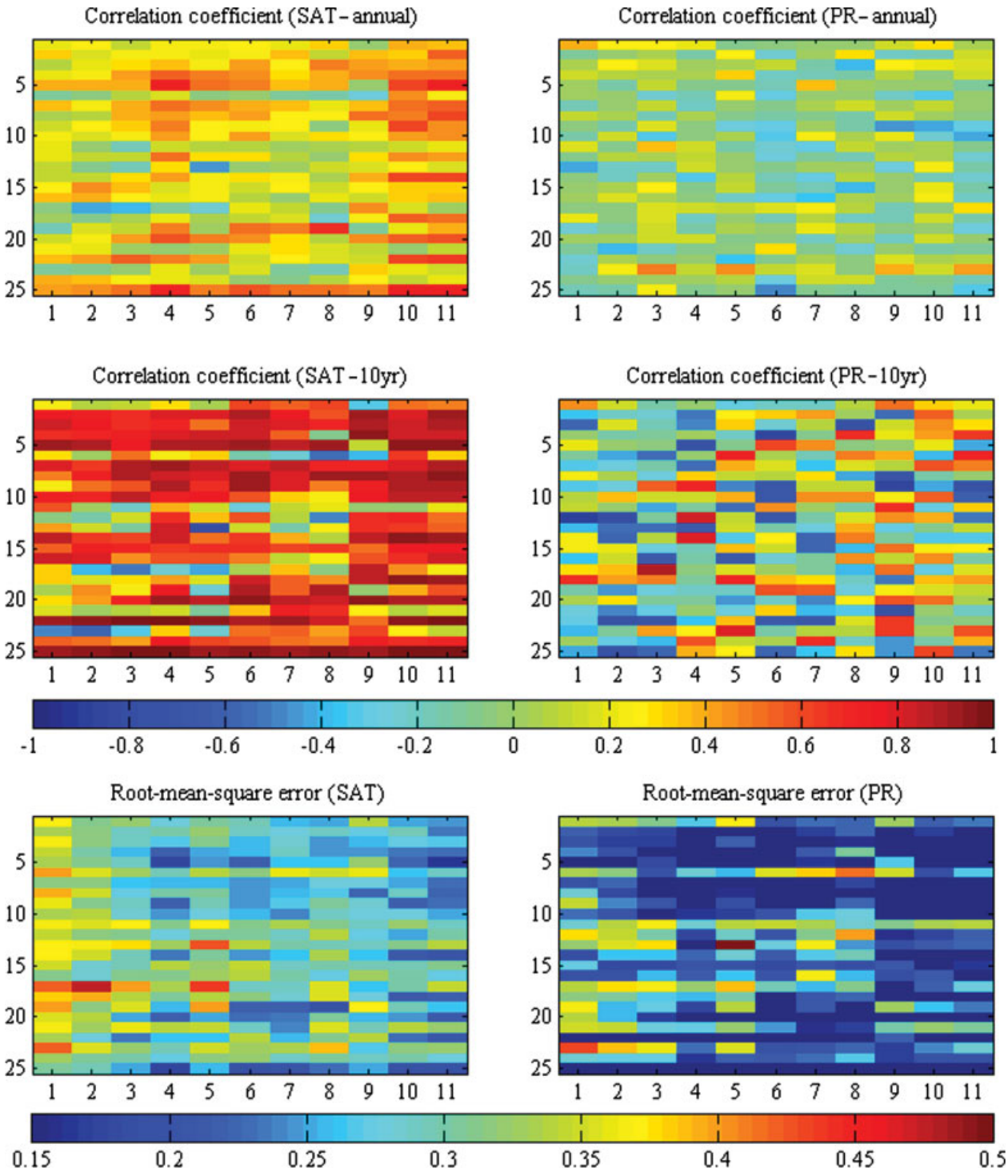

Figure 3. The performances of each single-model and multi-model ensemble outputs for annual simulation and 10-year moving average. The labels in horizontal axis indicate the regions, number 1–10 represent the ten river basins and number 11 represent China. The labels in vertical axis indicate the simulation results, numbers 1–24 represent the 24 single model, and number 25 is the REA results.

annual and 10-year moving average of SAT and PR are involved. For SAT, 10-year moving average SAT performs better than the annual SAT (higher R). In most models, R is >0.5. Moreover, the RMSE is primarily between 0.17 and 0.47; GCM5 (CNRM-CM5) and GCM6 (CSIRO-Mk3.6.0) perform better in most regions. The RMSE and R between SAT simulated by REA and observation are better in all river basins, indicating the improved performance on temporal scales. For PR, the calculated correlation coefficients are invariably <0.6 and the RMSEs are >0.23 in all regions compared with the observations. The results indicate the poor temporal performances for all models in simulating the annual PR. The ensemble method does not improve the performance

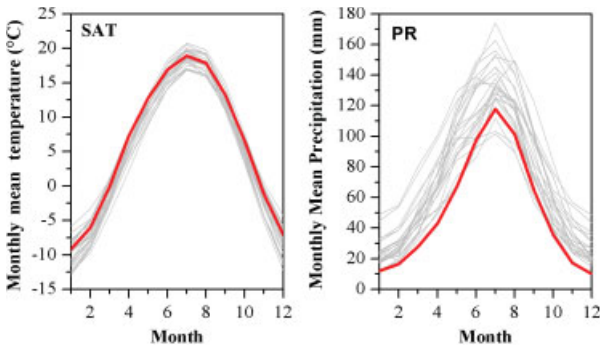

Figure 4. Annual cycles of monthly mean SAT (left) and PR (right) over China during the period 1970–1999. The thick black lines indicate the results of observation and each model simulation.

greatly. Overall, all models cannot accurately simulate the temporal PR and SAT characteristics in all river basins, and the performances are improved when facing decadal scale. Moreover, GCMs generally show better agreement with the observed SAT than PR; the GCMs are much less accurate at representing the annual variance than decadal variance.

Figure 4 compares the simulated monthly SAT and PR against the corresponding observations for the period 1970–1999, suggesting that the models are able to predict a realistic annual temperature and PR cycle. All models capture the monthly SAT profile characteristics. Most models underestimate monthly mean SAT, especially in winter. Generally, most models simulate the seasonal variation characteristics well with a single peak. The maximum PR is predicted during the monsoon season, except in GCM1 (BCC-CSM 1.1), GCM3 (BNU-ESM), GCM13 (HadGEM2-ES), GCM19 (MIROC-ESM-CHEM) and GCM24 (FGOALS-g2). However, nearly all GCMs overestimate the PR in all seasons. The simulated PR has a higher variation than the SAT variation.

3.1.2. *Spatial simulations*

Figure 5 shows the spatial distribution agreement between the observations and model simulation for the annual mean SAT and PR during the period 1970–1999. Compared with single-model predictions, the REA results generally perform better at simulating the spatial distributions, especially for PR. Figure 6 compares the spatial distribution of 30-year (1970–1999) average SAT and PR between observation and multi-model ensemble mean. The ensemble reproduces the important spatial temperature and PR characteristics in China, and the spatial correlation coefficients between the observations and ensemble mean are 0.85 and 0.81, respectively. Figure 6 also indicates the errors between the observations and REA results. For SAT, the REA results are higher relative to the observations over the mountain range along the mountainous areas in northwestern China, while cold biases are observed over northern and northwestern China, especially in the Tibetan Plateau. For PR, the positive PR error is largest across the mountainous areas in southwestern China and the Tibetan Plateau, whereas the negative error occurs in southeastern China.

3.2. SAT and PR projection in the 21st century

3.2.1. *Spatial patterns of climate change*

Figure 7 shows the spatial distribution of projected annual and seasonal temperature (linear trend) by using REA method for the period 2006–2099. Warming trends in the 21st century are identified over China in all emission scenarios. The range for these three scenarios is 0.02–0.78 °C decade^{-1}. The RCP 2.6 scenario, which represents the lowest RCP scenario assuming significant

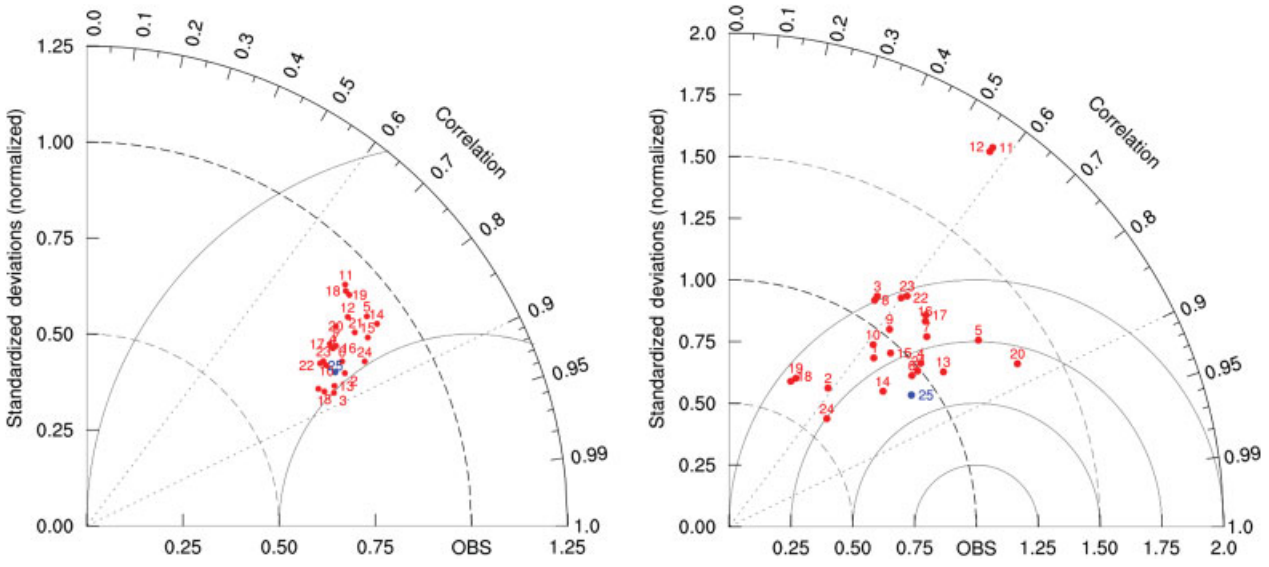

Figure 5. Taylor diagrams for the spatial distribution simulations of SAT (left) and PR (right). The coloured makers indicate the outputs of each model simulation (red) and the REA result (blue).

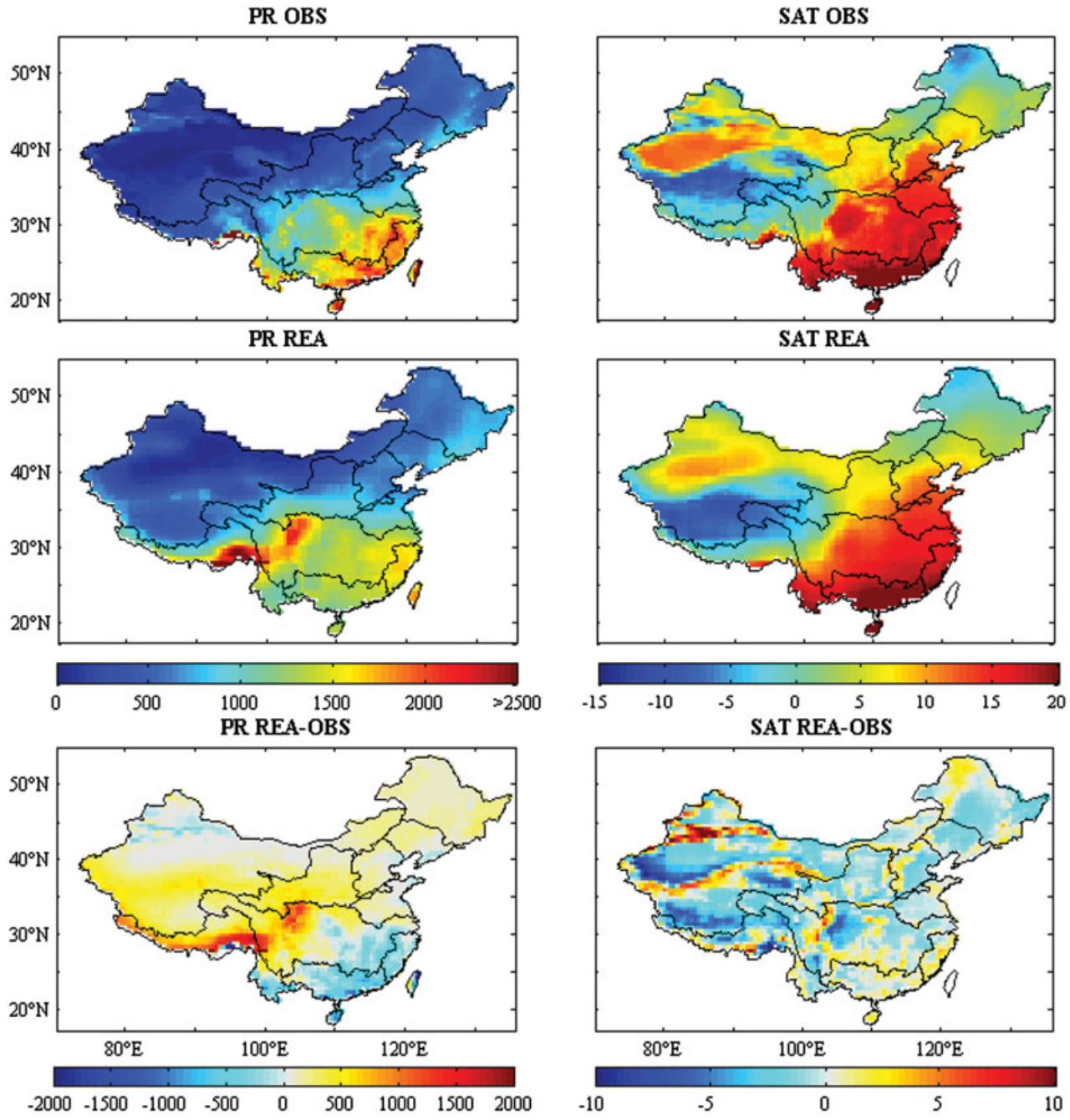

Figure 6. Spatial distribution of 30-year (1970–1999) average temperatures (°C) (left) and precipitation (mm) (right) based on the observation and REA results.

action to mitigate climate change (Rogelj *et al.*, 2012), has the smallest linear trend in SAT; the maximum trend is <0.15 °C decade^{-1}. RCP 8.5 represents a high-emission, non-mitigation future (Rogelj *et al.*, 2012) and yields the largest warming trend, i.e. >0.37 °C decade^{-1}. A range from 0.16 to 0.37 °C decade^{-1} is detected for the intermediate scenario RCP 4.5. The warming in northern China is more pronounced than southern China, especially under RCP4.5 and RCP 8.5, which are similar with observation and projection of models (Zhou and Yu, 2006; You *et al.*, 2014). Under RCP 4.5 and RCP8.5, the spring temperature shows relatively lower warming over nation. In northern China, including Songhua River, Liaohe River, Haihe River and Yellow River basin, the warming trend in December–January–February (DJF) is most pronounced. In southeastern China, including the middle and lower reaches of Yangtze River basin, Southeast River drainage system and Pearl River basin, the contribution to future warming in September–October–November (SON) is larger than that in other seasons. While in the Northwest River Drainage system, the projected temperature in June–July–August (JJA) shows higher linear trend. The warming in northern China is more pronounced than southern China, especially under RCP4.5 and RCP 8.5. Under RCP 2.6, the annual and seasonal trends in the upper Yangtze River basin, Southwest River drainage

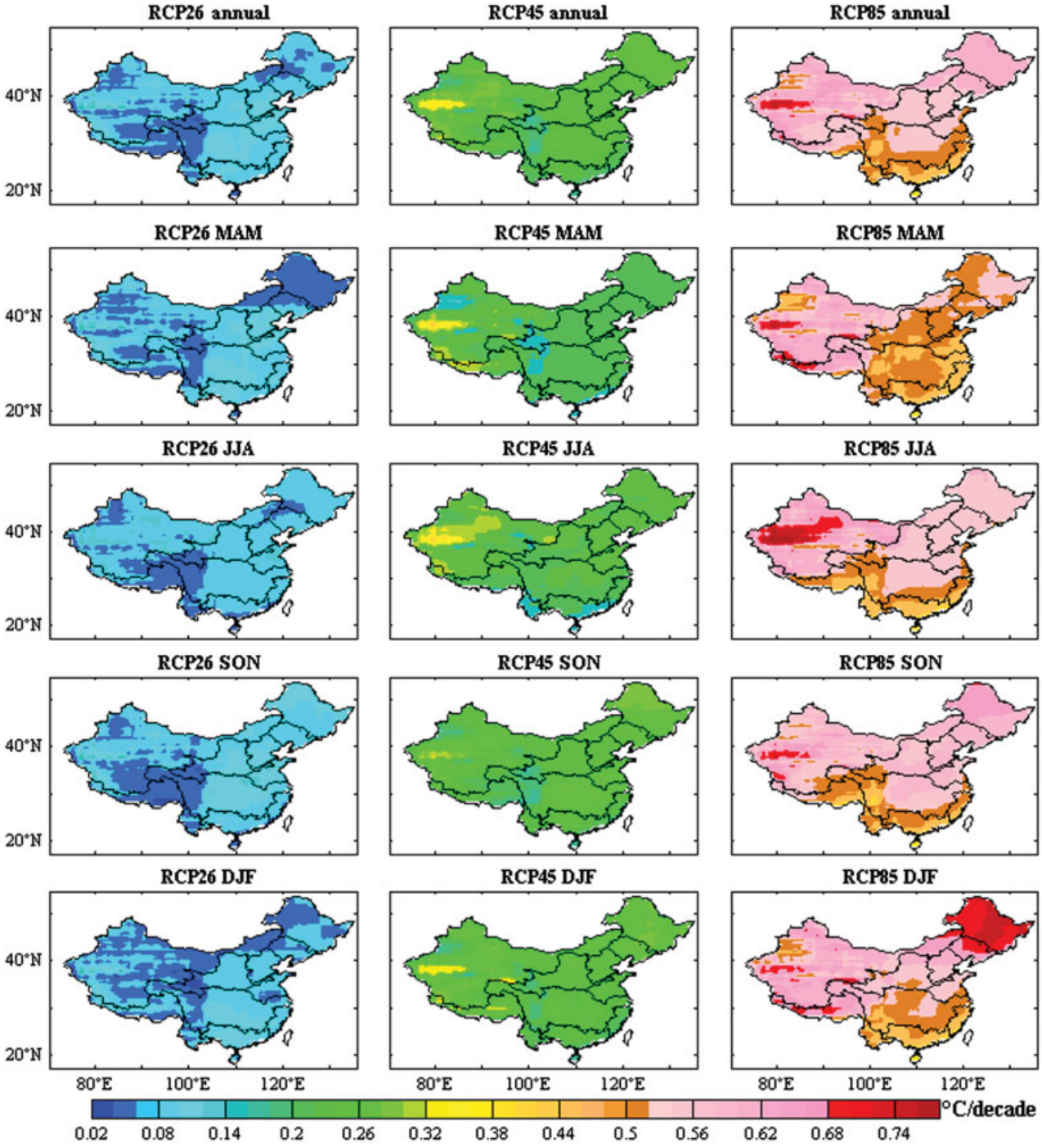

Figure 7. The decadal warming rates of projected SAT for the period 2006–2099 under the RCP 2.6, RCP 4.5 and RCP 8.5 scenarios.

system and southern of Northern River drainage system are not significant.

The spatial patterns of projected annual and seasonal PR changes under three emission scenarios are shown in Figure 8. The linear PR trends range from −10 to 20 mm decade^{-1}. PR increases nationwide in 21st century under all scenarios. The trends increase from western to eastern China, which is consistent with the previous study (Xu and Xu, 2012; Wang and Chen, 2013). The predicted trends are >10 mm decade^{-1} in eastern China; the largest trends are concentrated in the upper Yangtze River basin. Some areas have negative PR trends, primarily located in the central and southwest Northwest River drainage system. Seasonally, the spatial pattern of the PR change exhibits zonal characteristics. In Yangtze River basin and Huaihe River basin, the projected PR showed significant increasing trend in March–April–May (MAM) and JJA under all scenarios, but decreasing trend in SON under the RCP 8.5. The PR in MAM gave the greatest contribution to the future wetting in Yangtze River basin under all emission scenarios. PR in Southeast River drainage system, Pearl River basin and the lower of Southeast River

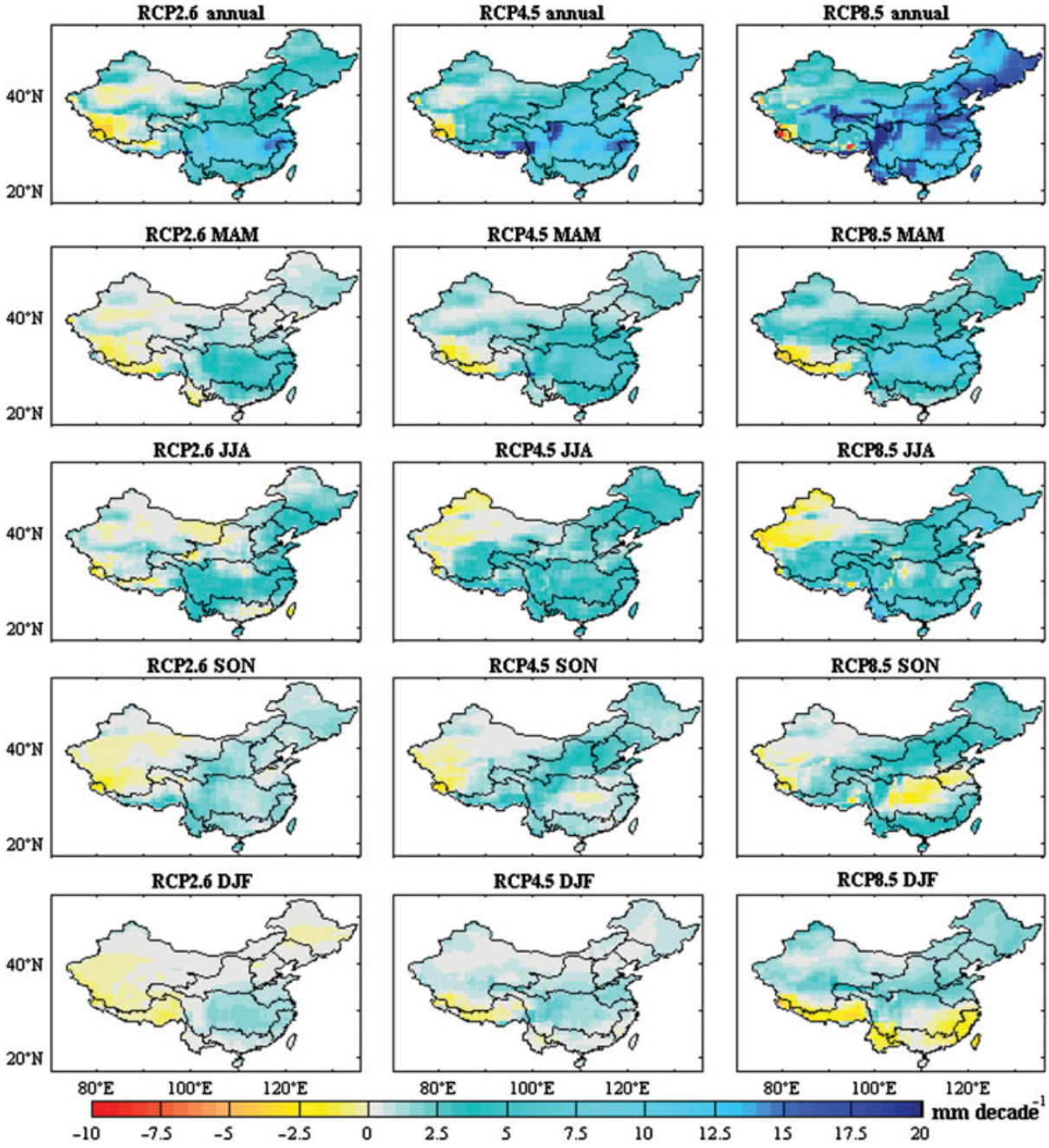

Figure 8. The decadal trends of projected precipitation for the period 2006–2099 under the RCP 2.6, RCP 4.5 and RCP 8.5 scenarios.

drainage system is projected to decrease in DJF. The main river basins in northern China showed positive trend in all seasons, and the contribution of JJA PR to annual PR increases is the largest. Summer PR in northern China is relatively higher than southern China, which indicates that the 'northern drying and south wetting' pattern observed in recent years (Ye *et al.*, 2013) may change in future under emission scenarios, especially under the RCP 8.5.

3.2.2. *Temporal trends of climate change*

The weight of each GCM was obtained using the REA method. And the projections for SAT and PR over the 21st century under different scenarios were generated based on the model's weights (Figure 9). The average SAT increases in the RCP 2.6, RCP 4.5 and RCP 8.5 scenarios are 0.87 ± 0.14 °C 100 year^{-1}, 2.47 ± 0.48 °C 100 year^{-1} and 5.85 ± 0.73 °C 100 year^{-1}, respectively. The changes in each scenario depend on the analysed period (Tables 2 and 3, and Figure 9). The three RCPs represent the different radiative forcings, energies and industrial CO_2 emission scenarios (Moss *et al.*, 2010; Taylor *et al.*, 2012). RCP 8.5 represents a 'high' emission scenario, and the radiative forcing in RCP 8.5 increases by approximately 8.5 W m^{-2} at the end of the 21st century (Taylor *et al.*, 2012). Therefore, the SAT increases the most in RCP

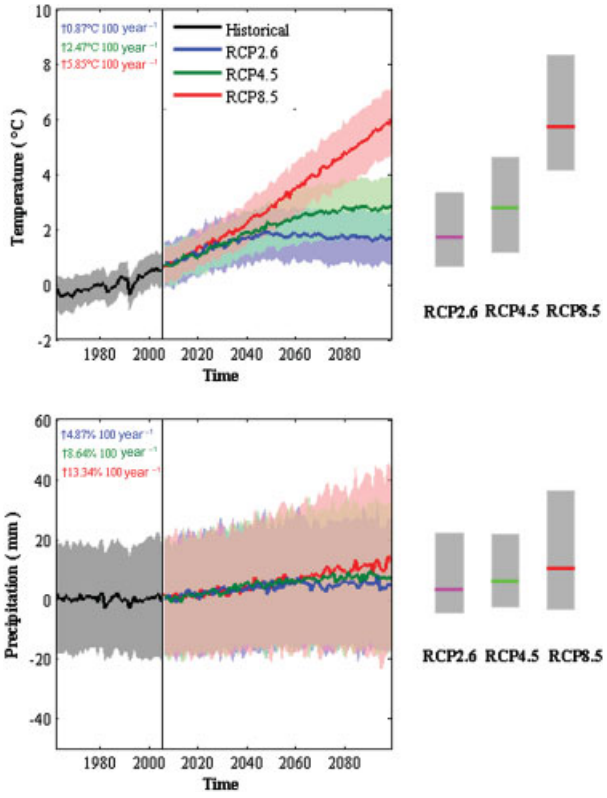

Figure 9. Ensemble results of annual mean SAT and annual mean PR in China during the period of 1962–2099 relative to 1970–1999. The thick coloured lines indicate the REA outputs in history (black) and RCP2.6 (blue), RCP4.5 (green) and RCP8.5 (red) scenarios. Shading denotes the ±1 standard deviation range of model annual averages. The grey bars in right of the figure represent the range of 24 model simulation estimations for the mean changes during 2090–2099. The coloured numbers indicate the linear trend of annual mean SAT and annual mean PR under different scenarios during the period 2006–2099.

8.5 and is higher for all periods compared with the other RCPs. The best SAT change estimate for RCP 8.5 is 5.73 °C by 2099 (the uncertainty range is 4.0–6.5°C). The RCP 4.5 scenario is a medium-mitigation emission scenario that stabilizes the direct radiative forcing at 4.5 W m^{-2} (~650 ppm CO_2 equivalent) at the end of the 21st century (Liu *et al.*, 2013). Under the RCP 4.5 scenario, the SAT change is less than for RCP 8.5, and the best SAT change estimate is 2.80 °C by 2099. In the early 21st century, SAT increases with the lowest rate. The SAT change for the period 2011–2030 is 1.20 °C, which is less than the predictions for RCP 2.6 (1.24 °C) and RCP 8.5 (1.36 °C) (Table 1). In the RCP 2.6 scenario, the radiative forcing reaches a maximum near the middle of the 21st century before decreasing to a nominal level of 2.6 W m^{-2} (Taylor *et al.*, 2012). This pathway represents a low so-called peak-and-decay scenario and yields distinct SAT change characteristics. The temperature also peaks in the mid-21st century, decreasing slightly thereafter. Thus, the average temperature is 1.86 °C for the period 2051–2070 and only 1.78 °C for the period 2071–2090. For RCP 2.6, the SAT increases by <2 °C by 2099; the best SAT change estimate is 1.71 °C.

Generally, PR increases during the 21st century under the RCP 2.6, RCP 4.5 and RCP 8.5 scenarios by $4.87 \pm 2.39\%$ 100 year^{-1}, $8.64 \pm 6.37\%$ 100 year^{-1} and $13.33 \pm 12.81\%$ 100 year^{-1}, respectively. It is also found that the projected PR under three scenarios increase for all periods (Table 3). Under the RCP 2.6 scenario, the largest PR change occurs in the period 2051–2070; the PR decreases slightly thereafter, which is similar to the temperature change. These results may provide evidence that PR and SAT are two important quantities with variations that are closely related via various physical processes (Wu *et al.*, 2013).

The projected SAT changes for the 21st century in the ten river basins are documented in Figure 10. The SAT change characteristics are similar to the features for China in all the three scenarios. It is clear that under both the RCP 4.5 and RCP 8.5 scenarios, the increase in the decadal mean SAT in the Songhua River vasin is the largest, increasing by 2.66 ± 0.49 °C 100 year^{-1} and 6.33 ± 0.82°C 100 year^{-1}, respectively. However, the largest warming trend occurs in the Huaihe River basin under the RCP 2.6 scenario. The SAT changes for different periods in the ten river basins are shown in Table 2. The SAT changes in the Southeast River drainage system and Pearl River basin are projected to change less than in the other basins for all periods, which are related to spatial pattern of temperature (Zhou and Yu, 2006).

Table 2. Decadal changes of projected temperature in ten river basins and China (unit: °C).

Basin	2011–2030			2031–2050			2051–2070			2071–2090		
	RCP2.6	RCP4.5	RCP8.5	RCP2.6	RCP4.5	RCP8.5	RCP2.6	RCP4.5	RCP8.5	RCP2.6	RCP4.5	RCP8.5
1	1.34	1.24	1.42	1.93	2.02	2.50	1.93	2.59	3.79	1.87	2.99	5.19
2	1.30	1.14	1.33	1.91	1.90	2.36	1.93	2.41	3.65	1.86	2.83	4.96
3	1.17	1.07	1.26	1.81	1.78	2.20	1.87	2.32	3.45	1.81	2.66	4.71
4	1.11	1.11	1.26	1.63	1.79	2.20	1.73	2.33	3.41	1.64	2.61	4.65
5	1.13	0.96	1.12	1.76	1.68	2.05	1.85	2.25	3.24	1.81	2.56	4.42
6	1.02	0.98	1.11	1.51	1.66	2.05	1.64	2.20	3.22	1.57	2.47	4.35
7	0.84	0.88	0.98	1.32	1.50	1.83	1.45	1.96	2.89	1.41	2.24	3.89
8	0.86	0.89	0.93	1.33	1.41	1.78	1.47	1.92	2.86	1.44	2.23	3.83
9	1.07	1.23	1.31	1.50	1.96	2.26	1.66	2.51	3.48	1.51	2.76	4.66
10	1.31	1.26	1.45	1.82	2.02	2.48	1.92	2.62	3.80	1.83	2.90	5.13
China	1.24	1.20	1.36	1.76	1.92	2.35	1.86	2.149	3.59	1.78	2.79	4.84

Table 3. Decadal changes of projected precipitation in ten river basins and China (unit: %).

Basin	2011–2030			2031–2050			2051–2070			2071–2090		
	RCP2.6	RCP4.5	RCP8.5	RCP2.6	RCP4.5	RCP8.5	RCP2.6	RCP4.5	RCP8.5	RCP2.6	RCP4.5	RCP8.5
1	4.83	4.37	5.49	7.85	8.45	7.77	8.81	11.77	12.19	9.50	12.23	17.69
2	5.62	4.50	5.17	8.13	10.53	8.60	11.91	14.39	14.34	11.83	13.104	18.96
3	6.29	4.90	5.26	8.88	10.33	8.69	11.12	12.34	14.99	10.76	14.49	17.89
4	2.72	2.37	2.59	4.74	5.62	5.29	6.88	7.24	10.10	5.27	9.78	13.62
5	0.99	1.42	2.04	4.15	4.20	4.28	6.03	6.03	8.72	4.94	7.87	12.16
6	−0.32	−0.41	−0.27	2.05	2.32	1.04	3.38	3.72	3.65	3.40	5.16	6.61
7	−1.46	−0.84	−1.79	0.87	0.30	−0.23	2.71	2.72	1.50	2.77	3.58	4.00
8	−0.33	−1.03	−1.98	1.74	2.15	0.23	1.95	3.25	1.81	2.34	4.28	5.67
9	−0.31	0.17	0.38	0.76	1.29	1.61	0.91	3.30	2.47	1.17	3.73	4.65
10	6.50	5.07	6.00	6.43	7.77	8.24	7.97	9.18	12.86	7.34	10.88	16.05
China	1.90	1.54	1.83	3.73	4..40	3.72	5.02	6.18	6.90	4.88	7.40	10.20

The projected PR changes for the 21st century in the ten river basins are depicted in Figure 11. During the 21st century, the results show that precipitation increases in all basins for RCP 2.6, RCP 4.5 and RCP 8.5. The rise in decadal regional mean PR in the Liaohe River basin is the largest under the RCP 2.6 and RCP 8.5 scenarios, changing by 8.57% 100 year^{-1} and 23.53% 100 year^{-1}, respectively. However, under the RCP 4.5 scenario, the Songhua River basin has the largest change, increasing by 11.73% 100 year^{-1}. The PR changes in the ten river basins have periodical features (Table 3). Compared with PR in baseline time (1970–1999), the river basins in northern China show more PR in all periods. In contrast, the Yangtze River basin, Southeast River drainage system and Pearl River basins show decreased PR for the period 2011–2030 under all scenarios. The decadal changes of PR in Yangtze River basin are consistent with the projection of CMIP3 under SRES (Tao *et al.*, 2012)

3.2.3. The uncertainties of temperature and precipitation change

Figures 9, 10 and 11 also show the uncertainty ranges of temperature and PR changes over China and ten river basins. The projected SAT uncertainty ranges generated by REA approach in the three future emission scenarios are similar. It is obvious that the range of 24 model simulation estimations (the grey bars in the right of figures) is larger than the uncertainty range obtained from the REA method for all the three scenarios (Figures 9 and 10). The uncertainties in projecting future temperature change can be partially reduced by applying the REA method. To quantify the model weights, REA method takes the performance of each model in representing the current climate and the convergence of its projection into account. Consequently, the outlier results are down weighted in the ensemble mean, and the magnitude of uncertainty range based on weights can be reduced to some extent (Torres and Marengo, 2013).

The uncertainties in the PR projection generated by the REA shows no marked improvement when compared with the range of 24 model simulation estimations (Figures 9 and 11). Thus, the uncertainty range cannot be narrowed using the REA method in all basins under the three scenarios. The magnitudes of uncertainty range are inconsistent among different basins. The uncertainty ranges has the same order of magnitude in the river basin over southern China, including Yangtze River basin, Pearl River basin, Southeast River drainage and Southwest River drainage system. Moreover, the uncertainty ranges are similar in all scenarios and time slices, which is in respond to the no significant change and large discrepancy under different scenarios. In the Liaohe River basin, Haihe River basin and Northwest River drainage system, larger magnitude of uncertainty ranges were detected. And the magnitudes increase with the time and emission scenarios.

4. Discussion and conclusions

The performances of 24 CMIP5 climate models in simulating PR and SAT variability in China and different river basins are evaluated. The projected climate changes for different scenarios over China and ten river basins according to the REA method, which is based on the multi-model ensemble, are described. The results show that most models underestimate the annual mean SAT in different river basins and China. Most models overestimate annual mean PR in China and the river basins in northern and western China, but underestimate the annual mean PR in the Pear River basin and Southeast River drainage system. It is in accordance with the overestimation for extreme PR in western and northern China, but underestimation for extreme PR in southern China (Ou *et al.*, 2013). Because China is a region with complex topography, i.e. the Tibetan Plateau is to the west and various mountain chains exist in the northern and central regions, climate in China is characterized by a large variability in space and time (Gao *et al.*, 2008). Therefore, all models cannot accurately simulate the temporal characteristics of PR and SAT in all climate regions. The GCMs generally show better temporal performances for SAT than PR. Precipitation variations are strongly influenced by vertical air movement due to atmospheric instabilities of various kinds and by the flow of air over orographic features (IPCC, 2007). Moreover,

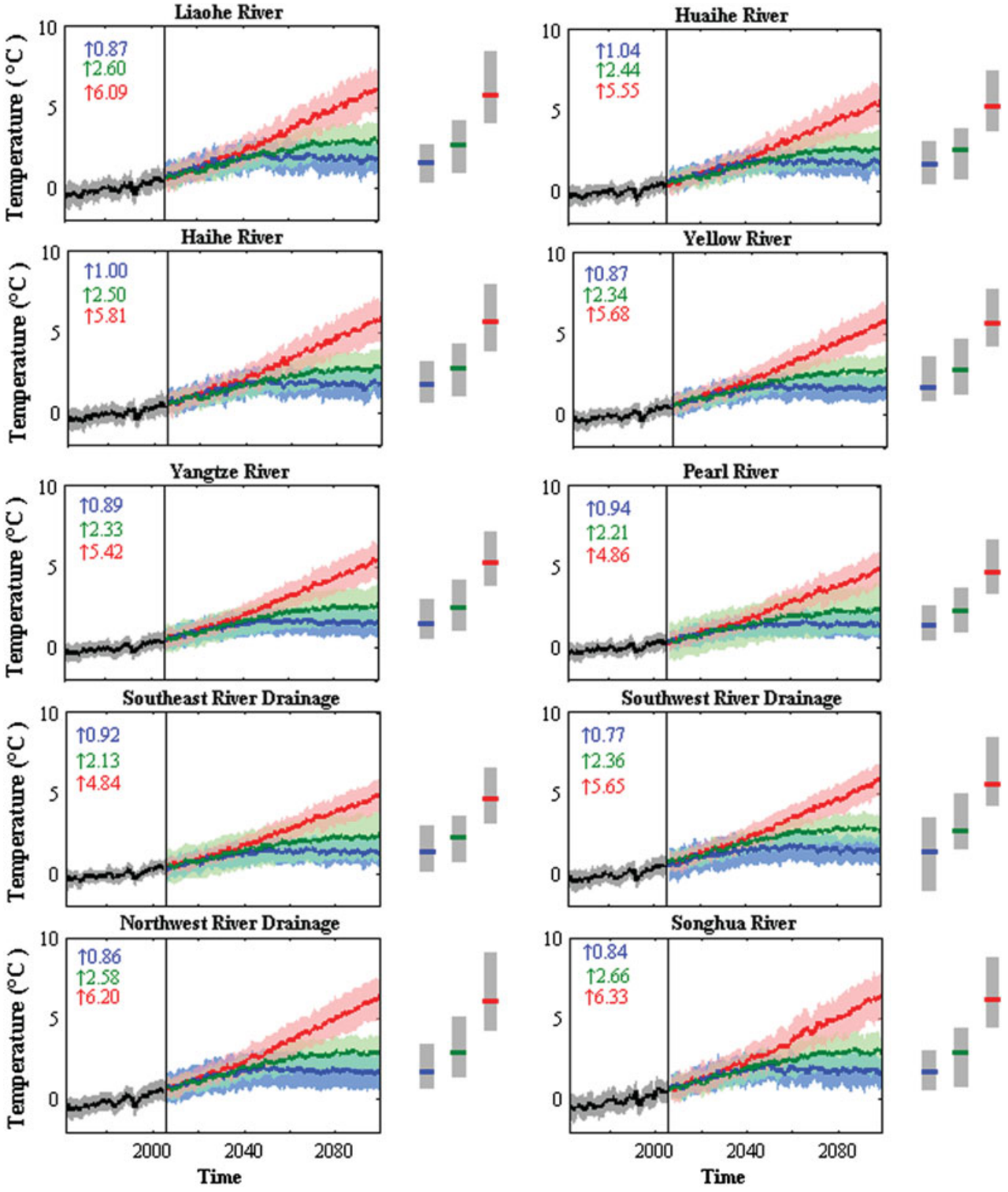

Figure 10. Ensemble results of annual mean SAT in the ten river basins during the period of 1962–2099 relative to 1970–1999. The thick coloured lines indicate the REA outputs in history (black) and RCP2.6 (blue), RCP4.5 (green) and RCP8.5 (red) scenarios. Shading denotes the ±1 standard deviation range of model annual averages. The grey bars in right of the figure represent the range of 24 model simulation estimations for the mean changes during 2090–2099. The coloured numbers indicate the linear trend of annual mean SAT under different scenarios, unit: °C 100 year^{-1}.

representing the inherent spatial variability and characteristics of precipitation in global climate models is also fraught with many difficulties (Stephens and Ellis, 2008). Moreover, the results indicate that models with higher resolution do not show better temporal performances in predicting SAT and PR than those with lower resolutions, which corroborates previous studies (Miao *et al.*, 2012a).

Under all RCP scenarios, warming trends in the 21st century appear over China. Overall, the northern regions exhibit a larger warming than the southern regions under

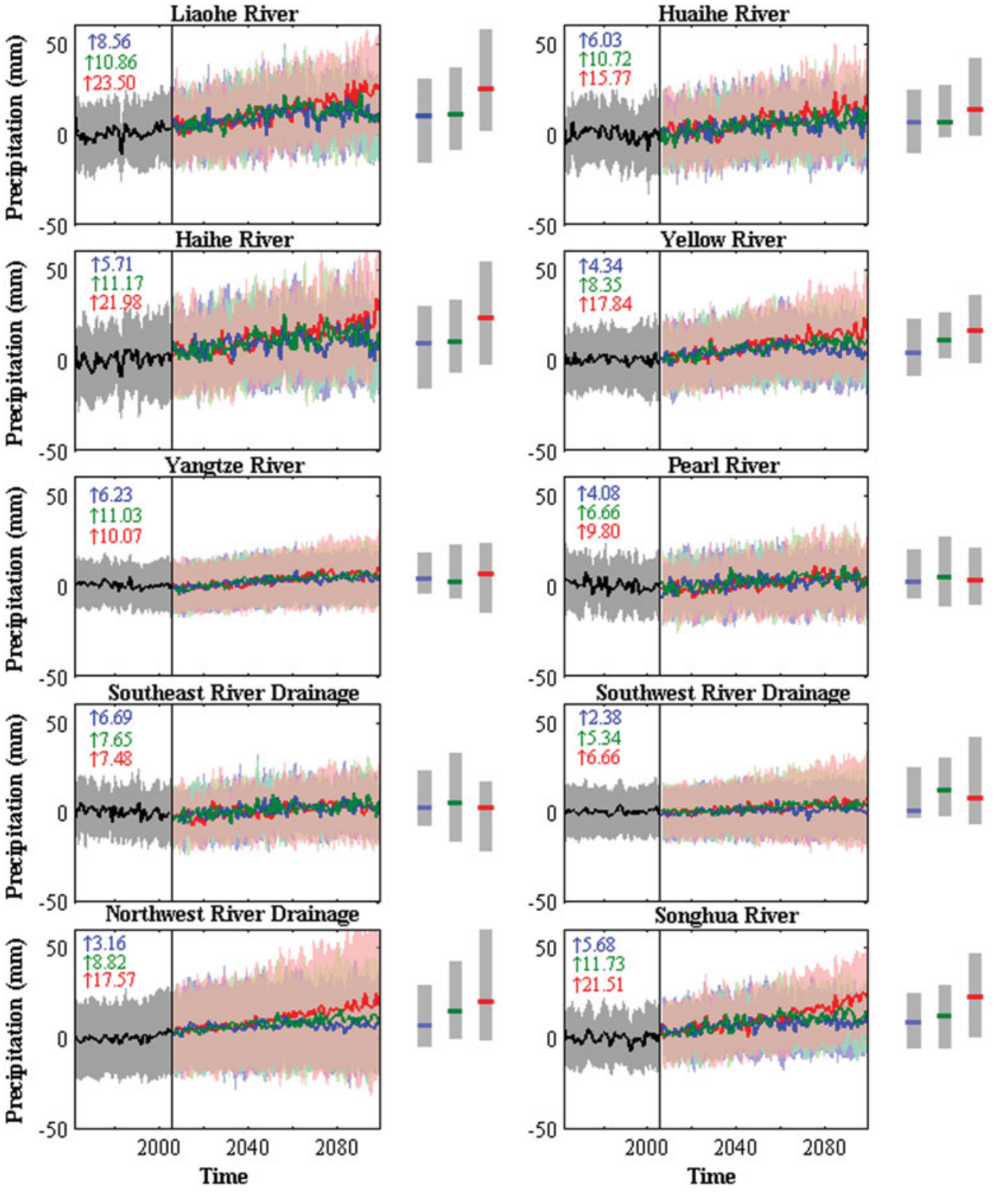

Figure 11. Ensemble results of annual mean PR in the ten river basins during the period of 1962–2099 relative to 1970–1999. The thick coloured lines indicate the REA outputs in history (black) and RCP2.6 (blue), RCP4.5 (green) and RCP8.5 (red) scenarios. Shading denotes the ±1 standard deviation range of model annual averages. The grey bars in right of the figure represent the range of 24 model simulation estimations for the mean changes during 2090–2099. The coloured numbers indicate the linear trend of annual mean PR under different scenarios, unit: %100 year^{-1}.

RCP 4.5 and RCP 8.5 on both annual and seasonal scales. Under the RCP 2.6 scenario, the warming trends in the eastern regions, especially in the Haihe River basin, Huaihe River basin and the central Yangtze River basin, are larger than in the western regions. For temporal scales, the warming trend from 2006 to 2099 in China is 0.87 ± 0.14 °C 100 year^{-1}, 2.47 ± 0.48 °C 100 year^{-1} and 5.85 ± 0.73 °C 100 year^{-1} for RCP 2.6, RCP 4.5 and RCP 8.5, respectively. The warming tendency for different periods is consistent with the different pathways that the RCPs

represent in terms of radiative forcing and energy and industrial CO_2 emissions. On regional scales, the temperature change characteristics in ten basins are similar to the general features of China. The Songhua River basin has the largest warming among the ten basins under the RCP 4.5 and RCP 8.5 scenarios. However, for RCP 2.6, the greatest warming trend occurs in the Huaihe River basin.

Precipitation in China is projected to increase by $4.87 \pm 2.39\%\ 100\,\text{year}^{-1}$, $8.64 \pm 6.37\%\ 100\,\text{year}^{-1}$ and $13.33 \pm 12.81\%\ 100\,\text{year}^{-1}$ for RCP 2.6, RCP 4.5 and RCP 8.5, respectively, during the 21st century. This result is consistent with the previous global precipitation predictions (Wentz *et al.*, 2007). The PR trends indicate that precipitation is sensitive to CO_2 emissions. The Yangtze River basin, Southeast River drainage system, Liaohe River basin, southern Songhua River basin and the lower reaches of the Southwest River drainage system are wetter in the 21st century for all scenarios. The maximum linear trends are concentrated in Yangtze River basin. Most of these river basins are located in eastern China. Therefore, the mean PR change over these regions may be affected by the monsoon circulation response to global warming, which determines the change in water vapour convergence over eastern China (Li *et al.*, 2011; Jiang and Tian, 2012). Moreover, some locations in the southwest and central Northwest River Drainage have negative PR trends under the RCP 2.6 scenario. For the regional mean PR, all basins are wetter by the end of the 21st century in all the three emission scenarios. However, PR tends to decrease in the Yangtze River basin, Southeast River drainage system and Pearl River basin for the early time period (2011–2030) under all RCPs, increasing substantially thereafter. This result is a response to the monsoon circulation. Sun and Ding (2009) suggested that the enhanced monsoon circulation will exhibit a two-stage evolution during the period 2010–2099 with a prominent increase after the 2040s.

Comparing this study to the previous studies, basically consistent conclusions are obtained for the spatial pattern and periodic characteristic of SAT and PR change in 21st century. Some inconsistencies occur in the seasonal changes. Previous study argued that the winter temperature change is larger than other season over China in future (Jiang *et al.*, 2008; Wang and Chen, 2013; You *et al.*, 2014). This study shows that winter temperature in northern China is most pronounced under RCP4.5 and RCP8. In southeastern China, the SON contribution to future warming is slightly larger than other seasons. While in the Northwest River drainage system, the projected temperature in JJA shows higher linear trend.

Besides global climate models, previous studies have also applied RCMs, with higher resolution, to project the climate change (Gao *et al.*, 2008; Gao *et al.*, 2012; Gao *et al.*, 2013; Zhou and Zhou, 2013). In contrast to the overestimation for PR of Yangtze River basin in GCMs, Zhou and Zhou (2013) showed that the RCM RegCM3 underestimates both total and extreme PR in the basin. As simulated by multi-model ensembles, a general cold bias is found over Tibetan Platau and warm bias in the northern of Songhua River basin from the RegCM4.0 simulation (Gao *et al.*, 2013). Regional mean PR increase over China for multi-model ensemble and RegCM4.0 under RCP4.5/RCP8.5 are 8.64%/13.34% and 6.3%/8.0% (Gao *et al.*, 2013) in 21st century, respectively. The difference in PR change between GCMs and RCM may be related to the broader areas with a decreased PR.

Faced with the realities of a changing climate, decision makers in a wide variety of organizations are increasingly seeking reliable quantitative climate predictions (Hawkins and Sutton, 2009). However, uncertainties are unavoidable for SAT and PR projections. The uncertainties in different scenario projections using the REA method are similar. By applying the REA method, the uncertainties in projecting future SAT change can be partially reduced. However, the uncertainty range for PR estimation cannot be narrowed using the REA method. The uncertainty ranges for PR in the Liaohe River basin, Haihe River basin and Northwest River drainage basin are larger than that in other basins. The PR uncertainty is much larger than for temperature. The uncertainty arises from three sources, namely model uncertainty, scenario uncertainty and the random, internal variability of climate (Hawkins and Sutton, 2009); model uncertainty is generally the dominant source of uncertainty for longer lead times (Hawkins and Sutton, 2010). Therefore, future research, particularly regarding model development, ensemble projections using more reliable GCMs and an analysis of narrowing uncertainties, is essential for a better understanding of future changes.

Acknowledgements

Funding for this research was provided by the National Natural Science Foundation of China (No. 41001153), the National Key Basic Special Foundation Project of China (No. 2010CB428402), the Beijing Higher Education Young Elite Teacher Project and the State Key Laboratory of Earth Surface Processes and Resource Ecology. We are grateful to the Program for Climate Model Diagnosis and Intercomparison (PCMDI) for collecting and archiving the model data, and to the Chinese National Meteorological Information Center and Climate Prediction Center, National Oceanic and Atmospheric Administration (NOAA) for collecting and archiving the observed climate data.

References

Allen MR, Stott PA, Mitchell JFB, Schnur R, Delworth TL. 2000. Quantifying the uncertainty in forecasts of anthropogenic climate change. *Nature* **407**: 617–620, DOI: 10.1038/35036559.

Annan JD, Hargreaves JC. 2010. Reliability of the CMIP3 ensemble. *Geophys. Res. Lett.* **37**: –L02703, DOI: 10.1029/2009GL041994.

Cong Z, Zhao J, Yang D, Ni G. 2010. Understanding the hydrological trends of river basins in China. *J. Hydrol.* **388**: 350–356, DOI: 10.1016/j.jhydrol.2010.05.013.

Coquard J, Duffy PB, Taylor KE, Iorio JP. 2004. Present and future surface climate in the western USA as simulated by 15 global climate models. *Clim. Dyn.* **23**: 455–472, DOI: 10.1007/s00382-004-0437-6.

Duan Q, Phillips TJ. 2010. Bayesian estimation of local signal and noise in multimodel simulations of climate change. *J. Geophys. Res.* **115**: D18123, DOI: 10.1029/2009JD013654.

Feng J, Lee DK, Fu C, Tang J, Sato Y, Kato H, McGregor JL, Mabuchi K. 2010. Comparison of four ensemble methods combining regional climate simulations over Asia. *Meteorol. Atmos. Phys.* **111**: 41–53, DOI: 10.1007/s00703-010-0115-7.

Gao X, Shi Y, Zhang D, Giorgi F. 2012. Climate change in China in the 21st century as simulated by a high resolution regional climate model. *Chin. Sci. Bull.* **57**: 1188–1195, DOI: 10.1007/s11434-011-4935-8.

Gao X, Shi Y, Song R, Giorgi F, Wang Y, Zhang D. 2008. Reduction of future monsoon precipitation over China: comparison between a high resolution RCM simulation and the driving GCM. *Meteorol. Atmos. Phys.* **100**: 73–86, DOI: 10.1007/s00703-008-0296-5.

Gao X, Wang M, Giorgi F. 2013. Climate change over China in the 21st century as simulated by BCC_CSM1.1-RegCM4.0. *Atmos. Oceanic Sci. Lett.* **5**: 381–386, DOI: 10.3878/j.issn.1674-2834.13.0029.

Giorgi F, Mearns LO. 2002. Calculation of average, uncertainty range, and reliability of regional climate changes from AOGCM simulations via the "reliability ensemble averaging" (REA) method. *J. Clim.* **15**: 1141–1158, DOI: 10.1175/1520-0442(2002)015<1141:coaura>2.0.co;2.

Giorgi F, Coppola E. 2010. Does the model regional bias affect the projected regional climate change? An analysis of global model projections. *Clim. Change* **100**: 787–795, DOI: 10.1007/s10584-010-9864-z.

Giorgi F. 2003. Probability of regional climate change based on the Reliability Ensemble Averaging (REA) method. *Geophys. Res. Lett.* **30**: 1629, DOI: 10.1029/2003GL017130.

Giraldo JD, García Galiano SG. 2011. Building hazard maps of extreme daily rainy events from PDF ensemble, via REA method, on Senegal River Basin. *Hydrol. Earth Syst. Sci.* **15**: 3605–3615, DOI: 10.5194/hess-15-3605-2011.

Grainger S, Frederiksen CS, Zheng X. 2013. Modes of interannual variability of Southern Hemisphere atmospheric circulation in CMIP3 models: assessment and projections. *Clim. Dyn.* **41**: 479–500, DOI: 10.1007/s00382-012-1659-7.

Hawkins E, Sutton R. 2009. The potential to narrow uncertainty in regional climate predictions. *Bull. Am. Meteorol. Soc.* **90**: 1095–1107, DOI: 10.1175/2009BAMS2607.1.

Hawkins E, Sutton R. 2010. The potential to narrow uncertainty in projections of regional precipitation change. *Clim. Dyn.* **37**: 407–418, DOI: 10.1007/s00382-010-0810-6.

IPCC. 1990. *Climate Change: The IPCC Scientific Assessment (1990)*. Cambridge University Press: Cambridge, UK.

IPCC. 2001. *Climate Change 2001: The Scientific Basis. Contribution of Working Group I to the Third Assessment Report of the Intergovernmental Panel on Climate Change*. Cambridge University Press: Cambridge, UK.

IPCC. 2007. *Climate Change 2007: The Scientific Basis. Contribution of Working Group I to the Fourth Assessment Report of the Inter-governmental Panel on Climate Change*. Cambridge University Press: Cambridge, UK.

Jiang D, Tian Z. 2012. East Asian monsoon change for the 21st century: results of CMIP3 and CMIP5 models. *Chin. Sci. Bull.* **58**: 1–9, DOI: 10.1007/s11434-012-5533-0.

Jiang Z, Zhang X, Wang J. 2008. Projection of climate change in China in the 21st century by IPCC-AR4 models. *Geogr. Res.* **27**: 787–799, DOI: 100020585(2008)0420787213.

Krishnamurti TN, Kishtawal CM, Zhang Z, LaRow T, Bachiochi D, Williford E, Gadgil S, Surendran S. 2000. Multimodel ensemble forecasts for weather and seasonal climate. *J. Clim.* **13**: 4196–4216, DOI: 10.1175/1520-0442(2000)013<4196:MEFFWA>2.0.CO;2.

Lambert SJ, Boer GJ. 2001. CMIP1 evaluation and intercomparison of coupled climate models. *Clim. Dyn.* **17**: 83–106, DOI: 10.1007/PL00013736.

Li H, Feng L, Zhou T. 2011. Multi-model projection of July–August climate extreme changes over China under CO_2 doubling. Part I: precipitation. *Adv. Atmos. Sci.* **28**: 433–447, DOI: 10.1007/s00376-010-0013-4.

Liu C, Zhang D, Liu X, Zhao C. 2012. Spatial and temporal change in the potential evapotranspiration sensitivity to meteorological factors in China (1960–2007). *J. Geogr. Sci.* **22**: 3–14, DOI: 10.1007/s11442-012-0907-4.

Liu J, Song M, Horton RM, Hu Y. 2013. Reducing spread in climate model projections of a September ice-free Arctic. *Proc. Natl. Acad. Sci. U.S.A.* **110**: 12571–12576, DOI: 10.1073/pnas.1219716110.

McAfee SA, Russell JL, Goodman PJ. 2011. Evaluating IPCC AR4 cool-season precipitation simulations and projections for impacts assessment over North America. *Clim. Dyn.* **37**: 2271–2287, DOI: 10.1007/s00382-011-1136-8.

Miao CY, Duan QY, Sun QH, Li JD. 2013. Evaluation and application of Bayesian multi-model estimation in temperature simulations. *Prog. Phys. Geogr.* **37**: 727–744, DOI: 10.1177/0309133313494961.

Miao CY, Duan QY, Yang L, Borthwick AGL. 2012a. On the applicability of temperature and precipitation data from CMIP3 for China. *PLoS One* **7**: e44659, DOI: 10.1371/journal.pone.0044659.

Miao CY, Yang L, Chen XH. 2012b. The vegetation cover dynamics (1982–2006) in different erosion regions of the Yellow River basin, China. *Land Degrad. Dev.* **23**: 62–71, DOI: 10.1002/ldr.1050.

Miao CY, Ni JR, Borthwick AGL, Yang L. 2011. A preliminary estimate of human and natural contributions to the changes in water discharge and sediment load in the Yellow River. *Glob. Planet. Change* **76**: 196–205, DOI: 10.1016/j.gloplacha.2011.01.008.

Miao CY, Ni JR, Borthwick AGL. 2010. Recent changes in water discharge and sediment load of the Yellow River basin, China. *Prog. Phys. Geogr.* **34**: 541–561, DOI: 10.1177/0309133310369434.

Moise AF, Hudson DA. 2008. Probabilistic predictions of climate change for Australia and southern Africa using the reliability ensemble average of IPCC CMIP3 model simulations. *J. Geophys. Res.* **113**: D15113, DOI: 10.1029/2007JD009250.

Moss RH, Edmonds JA, Hibbard KA, Manning MR, Rose SK, van Vuuren DP, Carter TR, Emori S, Kainuma M, Kram T, Meehl GA, Mitchell JF, Nakicenovic N, Riahi K, Smith SJ, Stouffer RJ, Thomson AM, Weyant JP, Wilbanks TJ. 2010. The next generation of scenarios for climate change research and assessment. *Nature* **463**: 747–756, DOI: 10.1038/nature08823.

Mote PW, Salathé EP. 2010. Future climate in the Pacific Northwest. *Clim. Change* **102**: 29–50, DOI: 10.1007/s10584-010-9848-z.

Ou T, Chen D, Linderholm HW, Jeong JH. 2013. Evaluation of global climate models in simulating extreme precipitation in China. *Tellus A* **65**: 19799, DOI: 10.3402/tellusa.v65i0.19799.

Phillips TJ, Gleckler PJ. 2006. Evaluation of continental precipitation in 20th century climate simulations: the utility of multimodel statistics. *Water Resour. Res.* **42**: W03202, DOI: 10.1029/2005WR004313.

Räisänen J. 2007. How reliable are climate models? *Tellus A* **59**: 2–29, DOI: 10.1111/j.1600-0870.2006.00211.x.

Reichler T, Kim J. 2008. How well do coupled models simulate today's climate? *Bull. Am. Meteorol. Soc.* **89**: 303–311, DOI: 10.1175/BAMS-89-3-303.

Ren M, Yang R, Bao H. 1985. *An Outline of China's Physical Geography*. Foreign Languages Press: Beijing.

Rogelj J, Meinshausen M, Knutti1 R. 2012. Globalwarming under old and newscenarios using IPCC climate sensitivity range estimates. *Nat. Clim. Change* **2**: 248–253, DOI: 10.1038/nclimate1385.

Scherrer SC. 2011. Present-day interannual variability of surface climate in CMIP3 models and its relation to future warming. *Int. J. Climatol.* **31**: 1518–1529, DOI: 10.1002/joc.2170.

Sillmann J, Kharin VV, Zhang X, Zwiers FW, Bronaugh D. 2013. Climate extremes indices in the CMIP5 multimodel ensemble: part 1. Model evaluation in the present climate. *J. Geophys. Res.* **118**: 1716–1733, DOI: 10.1002/jgrd.50203.

Stephens GL, Ellis TD. 2008. Controls of global-mean precipitation increases in global warming GCM experiments. *J. Clim.* **21**: 6141–6155, DOI: 10.1175/2008JCLI2144.1.

Sun QH, Miao CY, Duan QY, Kong DX, Ye AZ, Di ZH, Gong W. 2014. Would the "real" observed dataset stand up? A critical examination of eight observed gridded climate datasets for China. *Environ. Res. Lett.* **9**: 015001, DOI: 10.1088/1748-9326/9/1/015001.

Sun Y, Ding Y. 2009. A projection of future changes in summer precipitation and monsoon in East Asia. *Sci. China Earth Sci.* **53**: 284–300, DOI: 10.1007/s11430-009-0123-y.

Tao H, Gemmer M, Jiang J, Lai X, Zhang Z. 2012. Assessment of CMIP3 climate models and projected changes of precipitation and temperature in the Yangtze River Basin, China. *Clim. Change* **111**: 737–751, DOI: 10.1007/s10584-011-0144-3.

Taylor KE. 2001. Summarizing multiple aspects of model performance in a single diagram. *J. Geophys. Res.* **106**: 7183–7192, DOI: 10.1029/2000JD900719.

Taylor KE, Stouffer RJ, Meehl GA. 2012. An overview of CMIP5 and the experiment design. *Bull. Am. Meteorol. Soc.* **93**: 485–498, DOI: 10.1175/bams-d-11-00094.1.

Tebaldi C, Knutti R. 2007. The use of the multi-model ensemble in probabilistic climate projections. *Philos. Trans. R. Soc.* **365**: 2053–2075, DOI: 10.1098/rsta.2007.2076.

Torres RR, Marengo JA. 2013. Uncertainty assessments of climate change projections over South America. *Theor. Appl. Climatol.* **112**: 253–272, DOI: 10.1007/s00704-012-0718-7.

Wang L, Chen W. 2013. A CMIP5 multimodel projection of future temperature, precipitation, and climatological drought in China. *Int. J. Climatol.* **34**: 2059–2078, DOI: 10.1002/joc.3822.

Wentz FJ, Ricciardulli L, Hilburn K, Mears C. 2007. How much more rain will global warming bring? *Science* **317**: 233–235, DOI: 10.1126/science.1140746.

Wu R, Chen J, Wen Z. 2013. Precipitation-surface temperature relationship in the IPCC CMIP5 models. *Adv. Atmos. Sci.* **30**: 766–778, DOI: 10.1007/s00376-012-2130-8.

Xie P, Chen M, Yang S, Yatagai A, Hayasaka T, Fukushima Y, Liu C. 2007. A gauge-based analysis of daily precipitation over East Asia. *J. Hydrometeorol.* **8**: 607–626, DOI: 10.1175/JHM583.1.

Xu C, Luo Y, Xu Y. 2011. Projected changes of precipitation extremes in river basins over China. *Quat. Int.* **244**: 149–158, DOI: 10.1016/j.quaint.2011.01.002.

Xu C, Xu Y. 2012. The projection of temperature and precipitation over China under RCP scenarios using a CMIP5 multi-model ensemble. *Atmos. Oceanic Sci. Lett.* **5**: 527–533.

Xu Y, Gao X, Shen Y, Xu C, Shi Y, Giorgi F. 2009. A daily temperature dataset over China and its application in validating a RCM simulation. *Adv. Atmos. Sci.* **26**: 763–772, DOI: 10.1007/s00376-009-9029-z.

Xu Y, Gao X, Giorgi F. 2010. Upgrades to the reliability ensemble averaging method for producing probabilistic climate-change projections. *Clim. Res.* **41**: 61–81, DOI: 10.3354/cr00835.

Ye J, Li W, Li L, Zhang F. 2013. "North drying and south wetting" summer precipitation trend over China and its potential linkage with aerosol loading. *Atmos. Res.* **125**: 12–19, DOI: 10.1016/j.atmosres.2013.01.007.

You Q, Min J, Fraedrich K, Zhang W, Kang S, Zhang L, Meng X. 2014. Projected trends in mean, maximum, and minimum surface temperature in China from simulations. *Glob. Planet. Change* **112**: 53–63, DOI: 10.1016/j.bbr.2011.03.031.

Zhai J, Liu B, Hartmann H, Da Su B, Jiang T, Fraedrich K. 2010. Dryness/wetness variations in ten large river basins of China during the first 50 years of the 21st century. *Quat. Int.* **226**: 101–111, DOI: 10.1016/j.quaint.2010.01.027.

Zhou L, Zhou T. 2013. Near future (2016–40) summer precipitation changes over China as projected by a regional climate model (RCM) under the RCP8.5 emissions scenario: comparison between RCM downscaling and the driving GCM. *Adv. Atmos. Sci.* **30**: 806–818, DOI: 10.1007/s00376-013-2209-x.

Zhou T, Yu R. 2006. Twentieth-century surface air temperature over China and the globe simulated by coupled climate models. *J. Clim.* **19**: 5843–5858, DOI: 10.1175/JCLI3952.1.

